# Small-molecule inhibitors of nisin resistance protein NSR from the human pathogen *Streptococcus agalactiae*

Nicola Porta<sup>a</sup>, Julia Zaschke-Kriesche<sup>b</sup>, Benedikt Frieg<sup>c,d</sup>, Mohanraj Gopalswamy<sup>a</sup>, Aleksandra Zivkovic<sup>a</sup>, Manuel Etzkorn<sup>d,e,f</sup>, Holger Stark<sup>a</sup>, Sander H. J. Smits<sup>b,g</sup>, Holger Gohlke<sup>a,c,d\*</sup>

<sup>a</sup>Institute for Pharmaceutical and Medicinal Chemistry, Heinrich-Heine-Universität Düsseldorf, Universitätsstrasse 1, 40225 Düsseldorf, Germany.

<sup>b</sup>Institute of Biochemistry, Heinrich-Heine-Universität Düsseldorf, Universitätsstrasse 1, 40225 Düsseldorf, Germany.

<sup>c</sup>John von Neumann Institute for Computing (NIC), Jülich Supercomputing Centre (JSC), Forschungszentrum Jülich GmbH, Wilhelm-Johnen-Straße, 52425 Jülich, Germany.

<sup>d</sup>Institute of Complex Systems – Structural Biochemistry (ICS-6), Forschungszentrum Jülich GmbH, Wilhelm-Johnen-Straße, 52425 Jülich, Germany

<sup>e</sup>Institute of Physical Biology, Heinrich-Heine-Universität Düsseldorf, Universitätsstrasse 1, 40225 Düsseldorf, Germany

<sup>f</sup>JuStruct: Jülich Center for Structural Biology, Forschungszentrum Jülich, GmbH, Wilhelm-Johnen-Straße, 52425 Jülich, Germany

<sup>g</sup>Center for Structural Studies, Heinrich-Heine-Universität Düsseldorf, Universitätsstrasse 1, 40225 Düsseldorf, Germany.

Author ORCID

Nicola Porta: 0000-0002-6005-4372 Benedikt Frieg: 0000-0002-7877-0262 Holger Gohlke: 0000-0001-8613-1447

Keywords: antibiotic resistance, lantibiotics, nisin, screening, small-molecule inhibitors

\*Corresponding author.

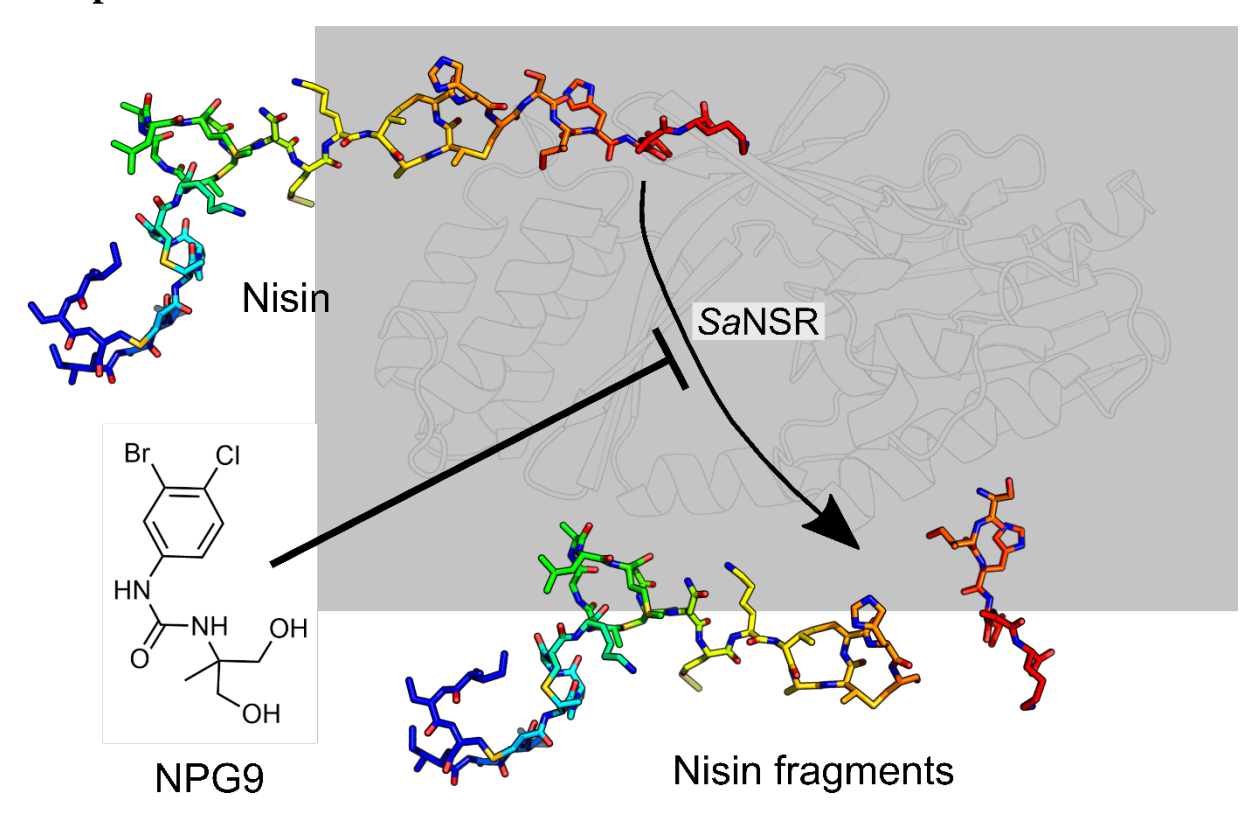
Address: Universitätsstr. 1, 40225 Düsseldorf, Germany.

Phone: (+49) 211 81 13662; Fax: (+49) 211 81 13847

E-mail: gohlke@uni-duesseldorf.de.

1

# **Graphical abstract**



Color should be used for any figures in print.

#### **Abstract**

Lantibiotics are antimicrobial peptides produced by Gram-positive bacteria and active in the nanomolar range. Nisin is the most intensely studied and used lantibiotic, with applications as food preservative and recognized potential for clinical usage. However, different bacteria that are pathogenic for humans and do not produce nisin, including *Streptococcus agalactiae*, show an innate resistance that has been related to the nisin resistance protein (NSR), a membrane-associated protease. Here, we report the first-in-class small-molecule inhibitors of *Sa*NSR identified by virtual screening based on a previously derived structural model of the nisin/NSR complex. The inhibitors belong to three different chemotypes, of which the halogenated phenyl-urea derivative NPG9 is the most potent one. Co-administration of NPG9 with nisin yields increased potency compared to nisin alone in *Sa*NSR-expressing bacteria. The binding mode of NPG9, predicted with molecular docking and validated by extensive molecular dynamics simulations, confirms a structure-activity relationship derived from the *in vivo* data. Saturation transfer difference-NMR experiments demonstrate direct binding of NPG9 to *Sa*NSR and agree with the predicted binding mode. Our results demonstrate the potential to overcome *Sa*NSR-related lantibiotic resistance by small molecules.

#### 1. Introduction

Without doubt, antibiotic resistance is one of the greatest health threats of our time. Misuse and overuse of antibiotics have accelerated the evolutionary selection process, which led to resistance against essentially all approved antibiotics [1]. Hence, there is an urgent need for antimicrobial compounds that can be used as alternatives to the classical antibiotic treatment. In this context, lantibiotics, a class of antimicrobial peptides, are attractive candidates due to their high activity against a wide range of Gram-positive human pathogenic bacteria [2, 3]. Peculiar post-translational modifications are contributing to the high thermostability and general stability against proteolytic degradation. Specifically, the enzymatic dehydration of Ser and Thr results in the formation of 2,3-dehydroalanine (Dha) and 2,3-dehydrobutyrine (Dhb) residues. Nucleophilic addition of the thiol group of a neighboring Cys residue then yields distinctive lanthionine (Lan from Dha) and methyllanthionine (MeLan from Dhb) rings, the presence of which is essential for the high antimicrobial potency [4].

Nisin is the most-studied lantibiotic and produced by a group of Gram-positive bacteria belonging to *Lactococcus* and *Streptococcus* species [5]. This 34 amino acids long cationic peptide is constituted of five lanthionine rings named A to E successively from the N- to the C-terminus. Since it was discovered in 1928 [6], it is one of the oldest known antibacterial agents. Nisin has been used widely as a food preservative, and initial therapeutic applications include human ulcer therapy and mastitis control in cattle [7]. Studies have reported that nisin can prevent the growth of drug-resistant bacterial strains, such as methicillin-resistant *Staphylococcus aureus* and *Clostridium difficile*. Increasing evidence indicates that nisin can also exhibit selective cytotoxicity towards cancer cells (for more details see review [5]). Its modes of action are related to the interaction with cellular membranes: for example specific binding of lipid II [8], thus inhibition of cell wall synthesis by interrupting peptidoglycan production [9], and formation of pores within the cell membrane that are made up of lipid II and nisin molecules [9, 10].

Due to their multiple modes of action, hardly any resistance against lantibiotics has developed over the past decades. However, different bacteria that are pathogenic for humans and do not produce nisin, including *Streptococcus agalactiae*, show an innate resistance that has been related to the nisin resistance protein (NSR), a membrane-associated protease [11, 12]. Specifically, NSR is a C-terminal processing protease belonging to the S41 family, as classified by MEROPS, the peptidase database [13]. The resistance mechanism involves enzymatic inactivation of nisin by cleavage of the last six residues. The resulting nisin fragment displays a up to 100-fold lower antibacterial efficacy and reduced affinity towards cellular membranes [14].

The crystal structure of NSR from *Streptococcus agalactiae* (SaNSR) was solved [15]. It contains an N-terminal helical bundle, and protease cap and core domains. The latter displays a region with the highly conserved TASSAEM sequence, with the previously identified catalytically active Ser236 [11]. The other residue constituting the catalytic dyad is His98, located between the helical bundle and the cap domain. Overall, the three domains constitute a hydrophobic tunnel of  $\sim 10$  Å width, and the protease cap forms a lid-like structure above it. By integrative modeling and mutagenesis studies a structural model of a nisin/SaNSR complex was generated that reveals that SaNSR recognizes the last C-terminal lanthionine ring of nisin, ring E [15]. This recognition determines the substrate specificity of SaNSR and ensures the exact coordination of the nisin cleavage site (peptide bond between MeLan28 in ring E and Ser29).

The identification of small-molecule inhibitors that interfere with SaNSR function is of utmost importance for making a therapy with nisin most effective. Here, we identified, by repetitive rounds of ligand- and structure-based virtual screening (Figure 1A), analogs search, and in vivo testing, inhibitors of SaNSR with different chemotypes. In order to prioritize molecules that resemble the recognition fragment of nisin and can inhibit SaNSR function, both shape matching and molecular docking were performed. In vivo validation of selected compounds revealed a selective functional inhibition towards SaNSR-expressing bacteria. To investigate NPG9 binding to SaNSR at the atomistic level, and further validate its binding mode, extensive molecular dynamics (MD) simulations of free ligand diffusion (fldMD) were performed. Finally, saturation transfer difference (STD) NMR experiments on NPG9 provide an additional validation of the binding mode from the biophysical point of view.

#### 2. Materials and Methods

#### 2.1 Preparation of nisin and SaNSR structures

The structures of nisin (extracted from PDB ID: 1WCO [10]) and SaNSR (PDB ID: 4Y68 [15]) were used for this study. In nisin, Asn27 was substituted by His to obtain a suitable nisin A structure from the crystallized nisin Z variant. SaNSR is a monomer in solution [15], therefore, only chain A was considered for further steps. Both structures were pre-processed with the Protein Preparation Wizard [16] of Schrödinger's Maestro Suite. Bond orders as well as missing hydrogen atoms were assigned, and the H-bond network was optimized. Finally, the systems were energy-minimized using the OPLS 2005 force field [17], resulting in a root mean square deviation (RMSD) of 0.3 Å with respect to the initial structure.

#### 2.2 Query generation

To screen for molecules with similar shape properties as the recognition region of nisin, we built a query for ligand-based virtual screening. To do so and to consider structural mobility, the nisin structure was subjected to all-atom MD simulations in explicit solvent, as reported previously [15], using Amber 16 [18]. Three independent trajectories of 500 ns length were analyzed with the cpptraj software [19]. To extract relevant conformations explored by nisin in solution, the MD-derived structural ensemble was clustered applying a hierarchical agglomerative approach. Prior to the clustering, conformations extracted every 5 ns were fit on the D ring region, using the first frame as reference, in order to remove global translation and rotation. As distance metric, the RMSD of backbone atoms was used, with a cutoff value for forming clusters of 4.5 Å. From the representative structures of the five most populated clusters, three different multi-conformation queries were built (Figure 1B) using ROCS [20]: I) based on rings DE, Ser29 and Ile30; II) based on rings DE only; III) based on ring E, Ser29 and Ile30.

#### 2.3 Virtual screening

A general workflow of the protocol used is reported in Figure 1A. Compounds were collected from ZINC15 [21] and eMolecules (https://www.emolecules.com) databases, which together

contain over 20 million molecules. For database preparation, including filtering and generation of up to 200 conformations per ligand, Omega [22] was used. In order to filter out compounds with unwanted pharmacokinetics, a drug-like filter was applied, and only compounds with logP < 6 and molecular weight (MW) between 200 and 600 Da were retained. A shape-based similarity search was then performed with the three shape queries generated above. Only the best fitting conformation for each compound was saved. The top 500 molecules for each query (1500 in total) were then docked into the *SaNSR* pocket using Glide [23] implemented in the Schrödinger's Maestro Suite 2017-1 (LLC, New York, NY, USA). A cubic grid of length 20 Å was centered on the catalytic residues His98 and Ser236. Compounds were first docked using Glide-SP (standard precision) protocol, and the 50% best-ranked were subsequently re-docked using Glide-XP (extra precision) protocol, which does more extensive sampling and uses a more sophisticated scoring function than the Glide-SP protocol. The best-ranked 750 compounds were then clustered with Canvas [24] based on 2D similarity (Tanimoto index calculated on MACCS keys fingerprint) and visually inspected, in order to select compounds with high diversity. At the end of this run, 11 compounds were purchased and tested.

The same protocol was applied a second time with additional filtering steps, in order to filter out structures with high complexity and those exhibiting non-lead-like properties: the first filter excluded compounds with more than five rings (RNG) and more than one chiral center (STER); the second is based on molecular descriptors related to lead structures [25], namely  $\leq 10$  rotatable bonds (RTB) and a MW  $\leq 460$  Da. This resulted in 23 compounds being purchased and tested.

Finally, considering preliminary *in vivo* data, a third group of compounds was selected based on the similarity with NPG9. An analogs search was performed focusing mainly on bioisosteric replacements of halogen atoms or variations of the two hydroxyl groups, resulting in the acquisition and testing of 12 derivatives.

#### 2.4 Molecular dynamics simulations

In order to investigate the recognition process and validate the predicted binding mode of inhibitors with SaNSR, a set of MD simulations was performed considering NPG9 as model inhibitor. NPG9 was optimized with Gaussian [26] at the Hartree-Fock level with the 6-31G\* basis set. Partial charges for each atom were derived with the RESP procedure [27], as implemented in Antechamber [28], by fitting to electrostatic potential grids generated by Gaussian. Different simulation systems of SaNSR and NPG9 were prepared for MD simulations with the LEaP program [29]. In particular, both the docking pose (P0, later referred to as "bound simulations") and ten random configurations of NPG9 relative to SaNSR (P1-P10, later referred to as "free ligand diffusion simulations", fldMD) were considered. In the first case, the structural stability of the complex and the diffusion of the ligand within the tunnel were analyzed. In the latter cases, the diffusion of the ligand was investigated aiming for reconstructing of the binding pathway of the SaNSR inhibitor. The ten random configurations were generated with packmol [30] with a minimum distance between NPG9 and SaNSR of 15 Å. Sodium counter ions were added to establish charge neutrality. Each system was placed in a truncated octahedral box of TIP3P water [31] with a minimum distance to the border of the box of 11 Å, resulting in a NPG9 concentration of ~1.4 mM. Structural relaxation, thermalization, and production runs of MD simulations were conducted with pmemd.cuda [32] of Amber 16 [18] using the ff14SB force field [33] for the protein, GAFF force field [34] for the ligand, and Joung-Chetham parameters for ions [35]. For each starting complex five independent replica of 500 ns length each were performed, resulting in a total of 50 simulations with a cumulative simulation time of 25 µs. Additionally, we performed MD simulations starting from the docked binding mode of NPG9 bound to *Sa*NSR. Again, five independent replicas of 500 ns length each were performed. In order to set up independent replicas and obtain slightly different starting structures, the target temperature was set to different values during thermalization (299.8 K, 299.9 K, 300.0 K, 300.1 K, 300.2 K and 300.3 K). A description of the thermalization protocol can be found elsewhere [36].

The analysis of the MD trajectories was carried out with cpptraj [19] on snapshots extracted every 1 ns. To measure structural mobility, we computed the residue-wise root mean square fluctuations (RMSF) of backbone atoms of SaNSR relative to the starting structure. To evaluate opening and closing of the cap domain, the distance between the centers of mass of the  $\beta$ -hairpin (262-TVNETFMLYDGARLALTTGIV-282) and the short loop regions of the protease core facing the tunnel (133-ISKL-136 and 135-TGGN-171) was computed. To investigate the molecular recognition of NPG9, the all-atom RMSD with respect to the ligand docking pose (RMSDd) or the previous frame (RMSDp) were computed. Cutoff values of RMSDd  $\leq 2.5$  Å and RMSDp  $\leq 2.5$  Å were used respectively to define binding on the protein surface (unspecific) and within the SaNSR tunnel (specific). Bound conformations were then clustered applying a hierarchical agglomerative approach and an RMSD cutoff value of 1.5 Å. Prior to the clustering, conformations were fit on the 10% least mobile residues of SaNSR, located in the protease core domain.

#### 2.5 Compound acquisition

The 46 selected compounds were either custom-synthetized or purchased from different suppliers as powder (Table S1). To ensure that there was no degradation of the compounds during the study, purity was re-assessed in a semi-quantitative way with LC-MS (exemplary cases are shown in Figures S4-S8; see also next chapter).

#### 2.6 Purity assessment with LC-MS

The compounds' stock solutions (~ 1 mg/ml in DMSO) were diluted with methanol hypergrade to concentrations of ~ 0.1-0.2 mg/ml. A volume of 2 μl was injected for each measurement. Relative purity of the compounds was determined as ratio of the area under the curve. LC system: Elute SP LC System (Bruker Daltonics, Bremen, Germany) with vacuum degasser, binary pump, autosampler, column oven. Column: Intensity Solo 2 C18 (100 mm \* 2.1 mm); Temperature: 50° C; Mobile phase: A. water hypergrade with 0.1 % formic acid (v/v) (Merck); B. Acetonitrile hypergrade (Merck); Flow Rate: 0.2 ml/min. Method 1: 0-4 min 95% A, 4-16 min gradient 95% to 5% A, 16-17 min gradient 5% to 0% A, reconditioning: 17-18 min gradient 0% to 95 % A, 18-21 min 95 % A. Method 2: 0-4 min 98 % A, 4-5 min gradient 98% to 95% A, 5-9 min 95% A, 9-16 min gradient 95% to 5% A, 16-17 min gradient 5% to 0% A, reconditioning: 17-18 min gradient 0% to 98% A, 18-21 min 98 % A. MS-System: amaZon speed ETD ion Trap LC/MSn System (Bruker Daltonics, Bremen, Germany); Ionisation:

electronspray; Polarity: positive; Alternating ion-polarity: on; Scan range: m/z: 80-1200; Nebulizer: Nitrogen, 15 Psi; Dry Gas: Nitrogen, 8 l/min, 200°C; Massrange mode: UltraScan.

#### 2.7 Cloning of the SaNSR protein

For studies in recombinant *Lactococcus lactis* cells, the plasmid pNZ-SV-SaNSR was obtained by cloning the gene nsr from *S. agalactiae* as previously described [11]. The plasmid was transformed using electrocompetent *L. lactis* NZ9000 cells. Therefore, a pulse setting of 1 kV, 25  $\mu$ F, 200  $\Omega$ , for 4.5-5.0 ms was used to electroporate the cells [37]. Afterwards, 950  $\mu$ l GM17 media was added, and the cells were incubated for 3 h at 30 °C. At last, the cells were plated on SMGG-agar plates containing 5  $\mu$ g/ml erythromycin. For STD-NMR studies, the plasmid pET-28b-SaNSR30-N8His was cloned as reported previously [38] and transformed into chemocompetent *E. coli* BL21 (DE3) cells using a 42 °C heat shock for 60 seconds. After 1 hour incubation at 37 °C, the cells were finally plated on LB-agar plates containing 30  $\mu$ g/ml kanamycin.

## 2.8 Expression and purification of the SaNSR protein

SaNSR30-N8His was expressed and purified as previously described [38]. Therefore, in *E. coli* BL21 (DE3) pET-28b-SaNSR30-N8His at an OD<sub>600</sub> of =0.8 to 1.0, the expression was induced with 1 mM IPTG and the cells were incubated overnight at 18°C with 160 rpm shaking. Subsequently, the cells were harvested and homogenized five times using 1.5 kbar (Microfluidics Homogenizer). After harvesting the cell debris at 42000 rpm for 45 minutes the supernatant was used for an ion metal affinity chromatography, using a HiTrap Chelating HP 5 ml column and an elution buffer containing 150 mM histidine. The eluted protein was further purified with a Superose 12 10/300 GL column, 25 mM MES pH 6 buffer with 150 mM NaCl.

#### 2.9 Purification of nisin

Nisin was purified with cation exchange chromatography as previously described [39]. To determine the concentration, the peptide was analyzed with RP-HPLC as previously described [40].

#### 2.10 Growth inhibition assay

*In vivo* validation of selected compounds was performed to test their ability to specifically inhibit the growth of *Sa*NSR-expressing strains. To do so, *L. lactis* cells grown in GM17 medium with 5 μg/ml erythromycin and 1 ng/ml nisin overnight. The cells were diluted in fresh media to an OD<sub>595</sub> of 0.1 and incubated for 30 min at 30 °C. In a 96 well plate, 50 μl of the selected compounds and the DMSO control (20%) were added. 150 μl of *L. lactis* NZ9000 pNZ-SV-Erm and *L. lactis* NZ9000 pNZ-SV-*Sa*NSR cells supplemented with 30 nM nisin, respectively, were added. After 5 hours at 30 °C the optical density was measured, and the relative growth inhibition was calculated by comparing the normalized values for *L. lactis* NZ9000 pNZ-SV-*Sa*NSR.

#### 2.11 Measurement of reduced nisin IC<sub>50</sub> values

In order to evaluate the inhibitory effect of the compounds, the reduced nisin IC<sub>50</sub> was measured as previously described [41]. In 96 well plates, a serial dilution of nisin was mixed with 150 μl of preincubated cells (OD<sub>595</sub> 0.1) containing 120 μM or 300 μM compound. The optical density was measured after 5 hours incubation at 30 °C and the IC<sub>50</sub> values were calculated. Reduced nisin IC<sub>50</sub> values were determined based on IC<sub>50</sub> values of the *Sa*NSR-expressing strain (*L. lactis* NZ9000 pNZ-SV-*Sa*NSR) with inhibitory compound compared to the same strain without compound and expressed as ratio of the two IC<sub>50</sub> values given in percent.

#### 2.12 Saturation transfer difference (STD) NMR experiments

As a biophysical validation of direct binding, STD NMR measurements were performed for the model inhibitor NPG9. This method allows identifying the binding of small ligands to macromolecules with dissociation constants  $K_D$  in the nM to mM range and characterizing the binding epitopes on the ligands [42, 43]. NMR experiments were recorded on a Bruker Avance III HD<sup>+</sup> 600 MHz spectrometer at 298 K in 100 mM sodium phosphate, 150 mM sodium chloride, 5% (v/v) DMSO, and 10% (v/v) D<sub>2</sub>O. Trimethylsilyl propionate (TSP) was used as an internal standard. STD NMR was performed with on-resonance protein saturation at 0.9 ppm using 2 s saturation time. Subtraction of the 1D STD spectrum was performed internally via phase cycling after every scan to minimize artefacts arising from temperature and magnet instability [42, 43]. The STD NMR experiment was carried out using 18  $\mu$ M of SaNSR protein and 1.8 mM of NPG9 compound. All NMR spectra were processed and analyzed with TOPSPIN 3.2 (Bruker).

#### 3. Results and Discussion

#### 3.1 Compounds selection

A hierarchical virtual screening protocol was applied to find small-molecules that inhibit SaNSR (Figure 1). Starting from a subset of drug-like molecules, using the free databases of commercially available compounds ZINC15 and eMolecules, 1500 compounds were selected based on shape similarity with nisin fragments involved in SaNSR recognition. In order to do so, rapid overlay of chemical structures (ROCS) [20] was applied for the calculation of 3D shape and chemical similarity. We built three queries, considering rings D and E as well as residues Ser29 and Ile30 (query I), rings D and E alone (query II), and ring E, Ser29 and Ile30 (query III) (Figure 1B). The selections were motivated by the fact that rings D and E form the recognition element of nisin at SaNSR and Ser29 and Ile 30 are in close proximity to the cleavage site (peptide bond between MeLan28 in ring E and Ser29) [15]. The best fitting compounds were submitted to molecular docking with Glide [23] in order to predict their configuration within the SaNSR binding site and to rank them according to the potential molecular interactions, as expressed by the docking score. The 750 molecules with the best docking scores were clustered and visually inspected, leading to the selection of 11 drug-like compounds for testing (NPG8 - NPG19, Table S1). In a second virtual screening run, two additional filtering steps were considered. The first filter excluded compounds with more than five rings (RNG) and more than one chiral center (STER). The second filter is based on molecular descriptors related to lead structures [25], namely  $\leq$  10 rotatable bonds (RTB) and a molecular weight (MW)  $\leq$  460 Da. After this run, 23 compounds were purchased and tested (NPG20 - NPG42, Table S1).

## 3.2 Biological activity

For experimental validation of the two groups of in total 34 compounds, a specific growth inhibition *in vivo* assay was performed, in which the selective inhibition towards *Sa*NSR-expressing *L. lactis* cells over *L. lactis* NZ9000 pNZ-SV-Erm containing an empty plasmid as control is probed utilizing a specific nisin concentration (30 nM). Specific growth inhibition is calculated as ratio between measured optical densities for the two strains and expressed as percentage. This assay was performed as a screening method, because *Sa*NSR-expressing bacteria are resistant against the nisin concentration used and growth is compared to the control strain; hence, only compounds inhibiting *Sa*NSR activity and making the bacteria more susceptible to nisin are identified.

Among the 34 compounds, three compounds showed a relevant inhibitory effect on SaNSR at the tested concentration of 150 µM (Table 1, Table S1). In particular, NPG9 inhibits bacterial growth by ~58 % in the presence of nisin as compared to control bacteria lacking SaNSR. Based on this, a third group of compounds was searched that are similar to NPG9 with respect to molecular recognition properties. For this, an analogs search was performed focusing on the following substitutions: bioisosteric replacement of halogen atoms with electron-withdrawing groups (e.g., cyano or trifluoromethyl groups [44]), substitution of the phenyl group with bulky hydrophobic moieties, or variations of the two hydroxyl groups. This step resulted in the selection of 12 derivatives (NPG43 - NPG55, Table S1; NPG53 was excluded from the study due to chemical stability issues). On this subset, as well as on NPG9 for comparison, in vivo validation was performed measuring reduced nisin IC<sub>50</sub> values. The reduced nisin IC<sub>50</sub> values denote nisin's potency from dose-response curves for the SaNSR-expressing strain in the presence of a fixed concentration of inhibitor, compared to the same strain without inhibitor; reduced nisin IC<sub>50</sub> values are expressed as the ratio between these two IC<sub>50</sub> values and given in percent. Hence, a strongly shifted dose-response curve towards the control strain NZ9000Erm, which is sensitive to nisin, indicates a higher inhibitory potency of the compound (Figure 2). To determine the inhibitory effect of the compounds, 120 µM and 300 µM were added to the assay with the SaNSR-expressing strain. Some compounds (e.g., NPG9) had a SaNSRindependent inhibitory effect on cell growth and could not be investigated at the higher concentration of 300 µM. Nisin IC<sub>50</sub> values are reduced by ~50% if NPG9 is used at 120 µM concentration (Table 1, Figure 2A), and by ~9 to 32% for NPG13, NPG24, NPG46 and NPG51 if these compounds are used at 300 µM concentration (Table 1, Figure 2B-C).

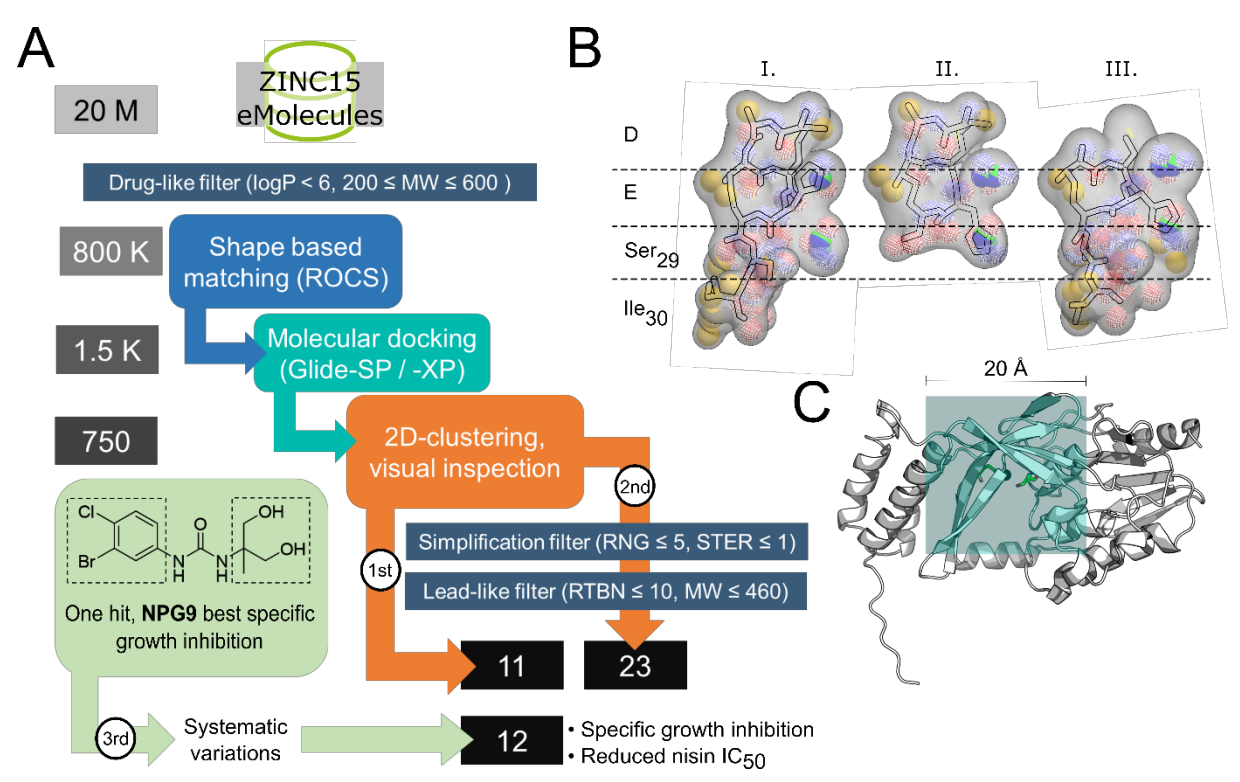


Figure 1. Virtual screening for SaNSR inhibitors. (A) Workflow for compound selection applied in this study. Shape-based matching followed by molecular docking and 2D clustering plus visual inspection led to the selection of in total 46 compounds for testing, 11 in the first round, additional 23 in the second round applying further filter criteria, and 12 more based on similarity to NPG9. These compounds were tested for growth inhibition in SaNSR-expressing cells and/or reduced nisin  $IC_{50}$ . On the left, the number of compounds considered in each step is indicated (K: indicates thousands; M: indicates millions). (B) Three queries generated for shape matching, based on varying nisin fragments including rings D and E, Ser29, and Ile30. For reasons of clarity, just one out of the five representative structures each is overlaid as sticks. The molecular shape is represented as a grey surface, while the chemical features are shown as spheres: H-bond acceptors as red grid, H-bond donors as blue grid, hydrophobic centers in yellow, rings and cations in green and blue, respectively. (C) Representation of the SaNSR structure used for docking (PDB ID: 4Y68) and the cubic grid centered on the catalytic dyad His98 and Ser236 (green sticks).

**Table 1.** Subset of compounds that showed SaNSR inhibitory activity<sup>a</sup>.

Internal ID, structure	Selection run	Specific growth inhibition <sup>b</sup>	Reduced Nisin IC₅₀ <sup>b</sup>	
		150 μM <sup>c</sup>	120 μΜ <sup>c</sup>	300 μM <sup>c</sup>
	1st	57.91 ± 1.72	50.5 ± 1.5	n.d.
	1st	16.89 ± 3.61		32.2 ± 5.0

2nd	20.66 ± 4.56	-	20.5 ± 12.1
3rd	-	8.1 ± 7.0	13.5 ± 6.4
3rd	-	4.0 ± 4.4	8.5 ± 5.8

<sup>a</sup>The full list of 46 tested compounds is shown in Table S1. Values were determined by at least three independent experiments. Measurements not performed are reported as "-". In cases where the compound was inhibiting the cell growth even without nisin, the measurement was marked as not determinable, "n.d.". Unless compounds are reported with explicit stereochemistry notation, the mixture of stereoisomers with undefined configurations was tested.

bIn %.

<sup>c</sup>Used compound concentration.

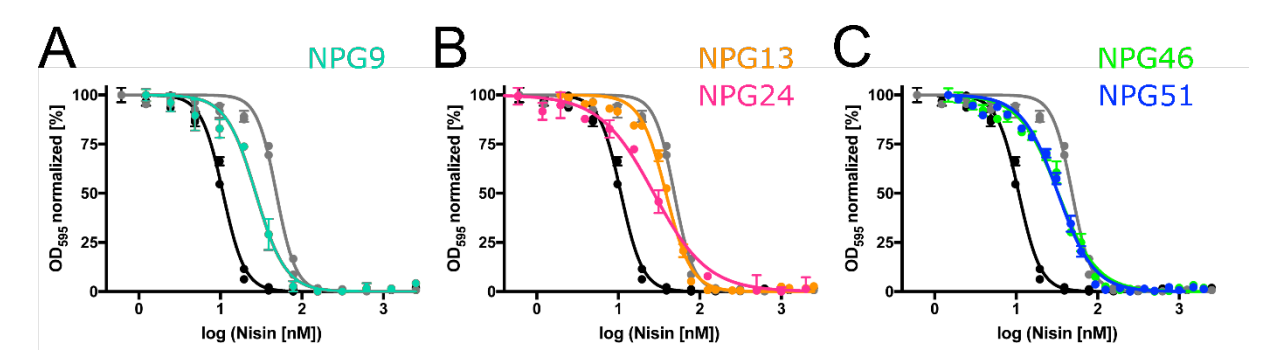


Figure 2. Determination of IC<sub>50</sub> values of nisin in the presence or absence of a SaNSR inhibitor. Doseresponse curves for SaNSR-expressing strain NZ9000SaNSR (in grey) and for the control strain NZ9000Erm (in black) are reported in comparison to SaNSR-expressing strain NZ9000SaNSR (A) with 120  $\mu$ M of NPG9 (in cyan), (B) with 300  $\mu$ M of NPG13 (in orange) and 300  $\mu$ M of NPG24 (in magenta), and (C) with 300  $\mu$ M of NPG46 (in green) and 300  $\mu$ M of NPG51 (in blue). The normalized measured OD<sub>595</sub> is shown in percentage against the logarithmic concentration of nisin. Values were determined by at least three independent experiments.

#### 3.3 Structure activity relationship (SAR) study

Most of the active molecules are linear, with one (e.g., NPG9) or two (e.g., NPG46) hydrophobic parts separated by an amide or urea linker. The presence of amide-like groups is not surprising because we searched for analogs of the peptide nisin. NPG13 displays a branching with an additional aromatic moiety (catechol) resulting in a T-shaped geometry.NPG24 is structurally different from the others, with pyrazolyl, 1,4-diazepanyl,

amide and cyclopropyl groups arranged in a linear fashion between two methoxyphenyl moieties. It displays weak growth inhibition and a moderately reduced nisin IC<sub>50</sub>, similarly to NPG13. Finally, NPG46 and NPG51, structural analogs of NPG9, display only very little reduced nisin IC<sub>50</sub> values (Tables 1, S1 and Figure 2). From the current data, a limited structure-activity relationship (SAR) can be derived (Figure 3): the minimal requirement for activity are a linear molecular shape and one or two hydrophobic regions separated by an amide-like group [45]. In nisin, MeLan and Ile residues represent these hydrophobic regions. Additionally, a hydroxyl group (e.g., NPG9) or an aromatic polar group (e.g., NPG13), matching respectively with Ser29 and His28 of nisin, can be present.

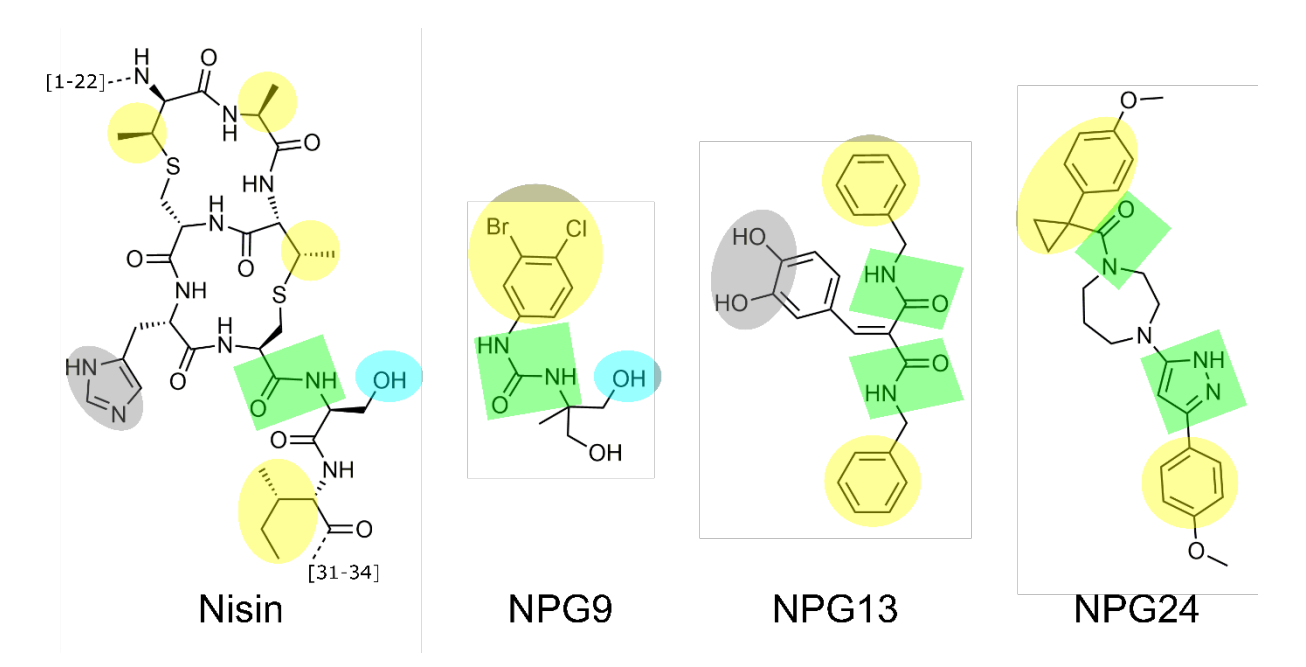


Figure 3. Chemical structures of the recognition region of nisin to SaNSR and compounds with SaNSR inhibitory activity. Fragments with similar properties are highlighted, with the nisin cleavage site (or amide-like groups) in green, hydrophobic moieties in yellow, hydroxyl groups in blue, and polar-aromatic groups in grey.

## 3.4 Binding mode prediction

This SAR derived from experimental data can be rationalized in terms of binding modes generated by molecular docking (Figure 4). In general, the binding mode of the compounds is consistent with the nisin/SaNSR model previously reported [15] in terms of location and orientation of the ligand within the SaNSR tunnel. As the binding mode prediction was done by molecular docking and, thus, independently from the ligand-based virtual screening, these findings implicitly validate the generated queries (Figure 1B). Additionally, the amide bond (or amide-like group [45]) is placed in-between the catalytic dyad, as found for the cleavage site of nisin [15]. More specifically, the hydrophobic regions of the ligands are consistently located in proximity of two hydrophobic patches within the tunnel, one formed by Val264, Tyr192, Ile202, Phe190, Met240 and Met173 in the upper region, and the other by Tyr261 and Ala235 close to the catalytic dyad. In both regions, most of the ligands (NPG9, NPG13, NPG24, NPG46) can perform favorable interactions with the  $\pi$ -electron systems of Phe190 and Tyr261 residues (also termed  $\pi$ - $\pi$  stacking). In the central portion of the tunnel, hydrophilic residues are prevalent instead, matching with the properties of the amide-like linker of the ligands: the linkers are involved in H-bond interactions with Gln100, Asn265, His98, Arg275, and Thr267

of the protease cap domain and Ser236, Ser237, Ser135, Thr169, and Gly171 of the core domain. Interestingly, in most of the compounds the amide-like group performs stabilizing interactions with the catalytic dyad of SaNSR. However, for NPG51 with a bulkier adamantyl substituent, there are no such favorable interactions, and  $\pi$ - $\pi$  stacking interactions are not possible either. Thus, sterically less demanding groups in the region mimicking the DE rings of nisin are apparently more favorable.

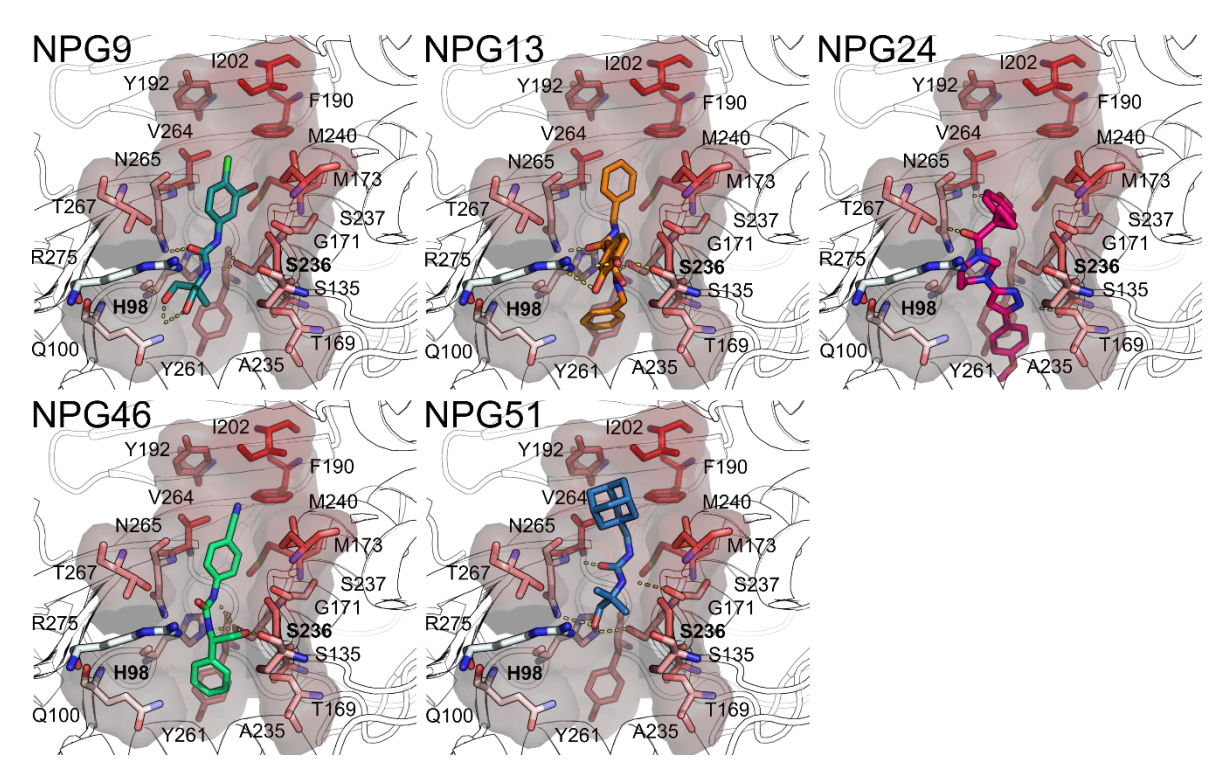


Figure 4. Binding modes generated by molecular docking of the subset of compounds that show SaNSR inhibitory activity (Table 1). Residues located at a distance  $\leq 4\text{Å}$  to the ligand are represented as surface-stick model, and the color scale from white to red represents increasing hydrophobicity of the residue (Eisenberg hydrophobicity scale [46]). The catalytically active His98 and Ser236 are highlighted in bold. H-bonds are shown as dashed lines. In the case of NPG46, only the S-stereoisomer with more favorable docking score is shown.

In order to investigate the recognition process and validate the predicted binding mode of SaNSR inhibitors, a set of MD simulations was performed, considering NPG9 as model inhibitor. In general, all-atom MD simulations are more detailed than molecular docking in that they allow to take into account protein mobility and to describe explicitly water molecules and ions. To ensure robustness of our results, multiple independent replica MD simulations were performed, for which NPG9 initially was either placed inside the protein binding site in the docked pose (five bound MD simulations starting from P0) or at ten randomly chosen positions in the solvent surrounding SaNSR (50 fldMD simulations, five replicas from each position P1-P10). In fldMD simulations, protein and ligand molecules interact in an unbiased manner, allowing to investigate in atomistic detail association and dissociation processes.

Analysis of SaNSR motions reveals for fldMD simulations that the N-terminus, helical bundle, and cap domain are most mobile, while the core domain and C-terminus are rather immobile (Figure S1A). As the cap domain constitutes part of the SaNSR tunnel, its movements lead to SaNSR exploring both open and closed states (Figure S1D). Still, even for fldMD simulations, the closed state is present in less than 1/6 of the cases (Figure S1-D, two replicas with > 75 %

and six with 75-50 % closed frames). Thus, even when starting from unbound *Sa*NSR, the tunnel is frequently accessible for the ligand.

To quantify ligand binding, as done previously [47], the RMSD, as measure of the average distance between atoms of different configurations, was calculated (Figures 5 and S2A). Each frame was therefore compared with the docked ligand pose (giving a RMSD<sub>d</sub> value) and with the previous frame in the trajectory (giving a RMSD<sub>p</sub> value) (Figure S2A). The first measure indicates (specific) binding to the tunnel (applying an RMSD<sub>d</sub>  $\leq$  2.5 Å, meaning high similarity with the docked ligand pose); if this is not given, the second measure indicates unspecific binding to the protein surface (applying an RMSD<sub>p</sub>  $\leq 2.5$  Å, meaning low variability in ligand's coordinates over time). MD simulations originating from the NPG9 docked pose revealed in general a stable binding mode, except in two cases where the ligand diffuses in the direction of a hydrophobic region formed by Tyr192, Ile202, and Phe190, which may be linked to a weak binding affinity; still, the ligand does not leave completely the tunnel (Figures S2B-C). During the 50 fldMD simulations, the ligand is in contact with the protein in ~75% of the frames (unspecific binding; Figure S3 and Table S2). Yet, clusters C3 and C6, which contain together 18% of the frames, represent NPG9 conformations that are in very good agreement with the docked NPG9 pose (Figure S3), as indicated by RMSD<sub>d</sub>  $\leq 2.5$  Å of the cluster representatives. Analysis of the time series of RMSD<sub>d</sub> values along all 50 fldMD simulations furthermore shows that such binding events occur across 11 different trajectories (Figure S2D): in three of them bound frames represent 10-50 % of the total ones, and in one replica even > 50% (Figure 5). In some trajectories, the bound pose (configurations with RMSD<sub>d</sub>  $\leq 2.5$  Å) is reached in  $\sim 100$  ns of simulation time (Figure 5, P2-II and P6-II), while in others it is reached after more than 400 ns (Figure 5, P4-II and P8-III). In both cases, the ligand stays bound for the remainder of the simulation time. Finally, in three out of the four cases, the ligand enters the tunnel from the entrance closer to the catalytic dyad (Figure 5, P2-II, P4-II and P6-II), suggesting that this may be the preferential access pathway. Overall, the fldMD simulations thus confirm the docked binding pose in an independent manner, which lends support to the above structure-based rationalization of the SAR.

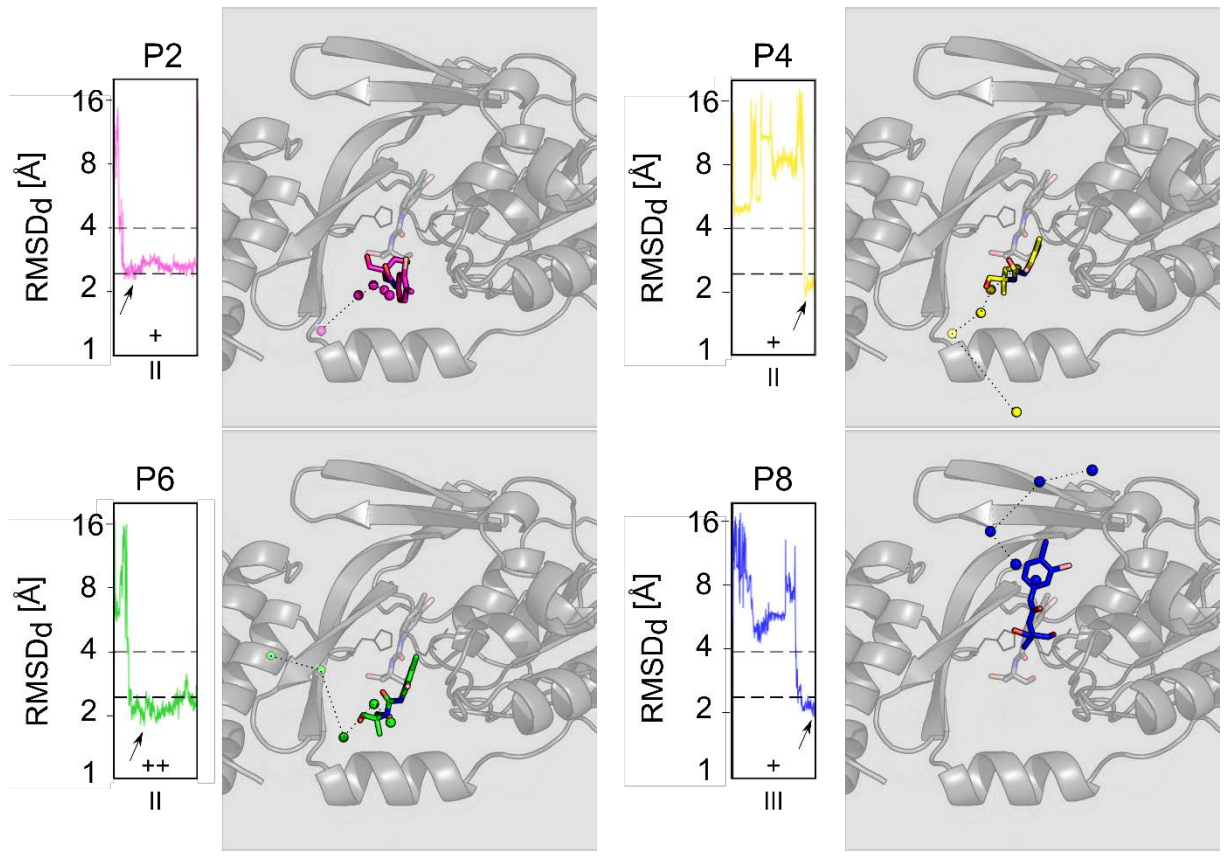
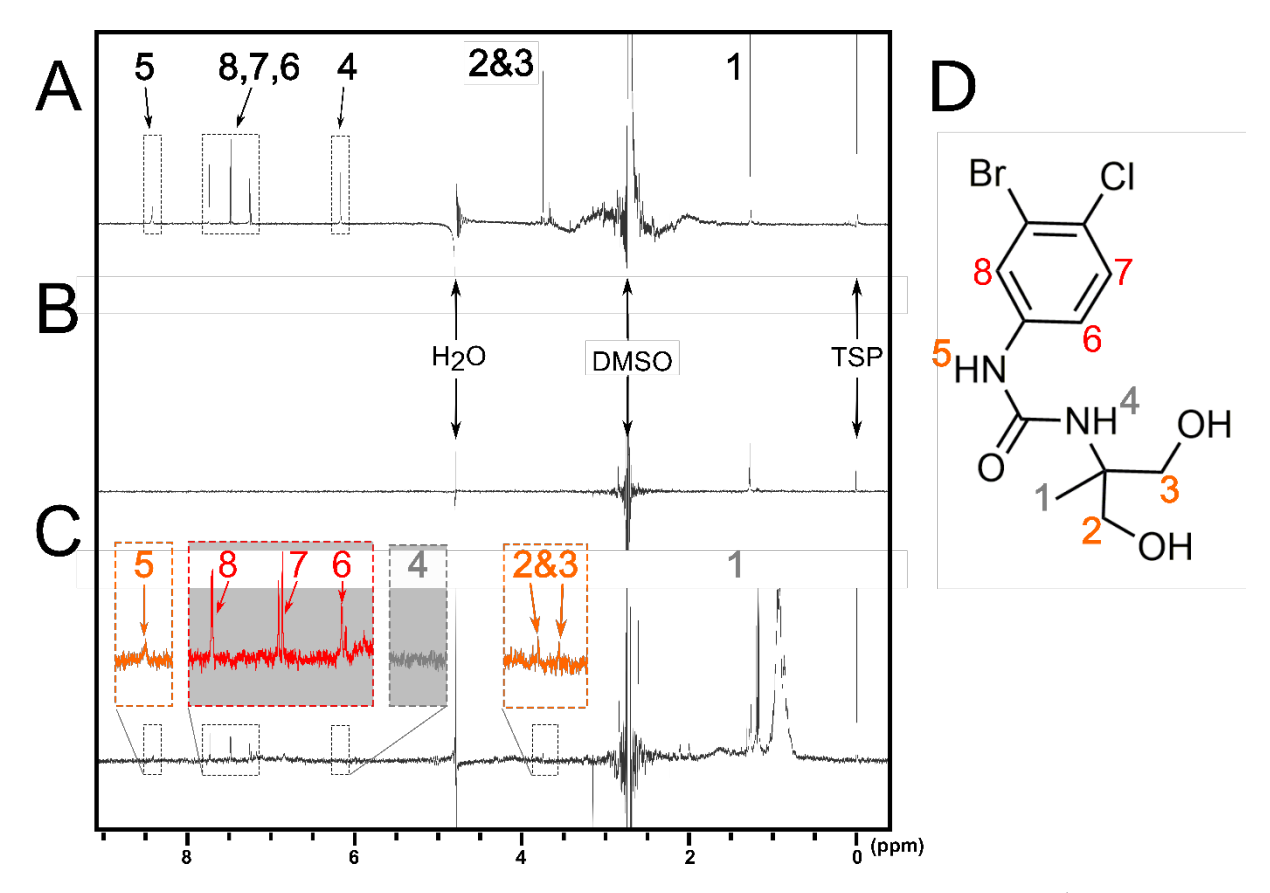


Figure 5. Analysis of NPG9 binding events for selected replicas of MD simulations. RMSD<sub>d</sub> time evolution of NPG9 during the fldMD simulations replicas with 10-50 % and > 50% bound frames (RMSD<sub>d</sub>  $\leq$  2.5 Å), marked with "+" and "++", respectively. Dashed lines representing the cutoff values for binding (2.5 Å, in black) and for pre-bound states within the tunnel (4 Å, in grey) are given. Each box with roman numbers represents a replica of 500 ns length; P2, 4, 6, and 8 denote the random starting position of the ligand. The arrow highlights the frame with lowest RMSD<sub>d</sub>, whose configuration is depicted (in color) and overlaid to the docking pose (in grey) within the *Sa*NSR binding site. The positions of the ligand in previous frames are also reported in terms of the centers of mass (spheres) in order to show the path leading to a bound state. Figure S2D shows the binding events for all the replicas of MD simulations performed.

#### 3.5 Biophysical validation

Finally, for NPG9, STD NMR experiments were performed (Figure 6). The most intense STD NMR signals are observed for aromatic protons, and weaker signals for one NH proton and the aliphatic CH<sub>2</sub> protons are detected. Due to an experimental artefact, CH<sub>3</sub> protons were not considered [48]. These results demonstrate that the ligand is binding to *Sa*NSR and are consistent with our binding mode model according to which the phenyl ring of NPG9 make interactions with *Sa*NSR (Figure 4).



**Figure 6. STD NMR of compound NPG9 in complex with** *Sa***NSR.** (**A**) Reference 1D <sup>1</sup>H NMR (STD-off) spectrum and STD spectrum of a sample containing 1.8 mM of NPG9 compound (**B**) without and (**C**) with 18 μM of *Sa*NSR protein. Assignment of the individual peaks for NPG9 is indicated by numbers from 1 to 8, color-coded according to the relative intensity of the STD signal from NPG9 protons. Strong signals (red) for aromatic (positions 6, 7, and 8) and weak signals (orange) for one NH (position 5) and aliphatic CH<sub>2</sub> protons (positions 2 and 3) were detected, which correlate with the proximity to *Sa*NSR. Methyl protons (position 1) are affected by irradiation power spillover (as visible by strong signal in the absence of *Sa*NSR protein in panel B), and one NH signal is not visible (position 4) (both grey colored).

#### 4. Conclusions

In conclusion, we identified the first-in-class small-molecule inhibitors of *Sa*NSR, belonging to three different chemotypes, of which the halogenated phenyl-urea derivative NPG9 is the most potent one. So far, no other biological activities have been reported for these compounds [49]. Co-administration with nisin yields increased potency compared to nisin alone in *in vivo* experiments with *Sa*NSR-expressing bacteria. The minimal requirement for activity are a linear molecular shape and one or two hydrophobic regions separated by an amide-like group. STD NMR experiments demonstrate direct binding of NPG9 to *Sa*NSR and are in accordance with a predicted binding mode. Together, these findings make these compounds interesting for further investigations, towards generating more potent inhibitors to overcome *Sa*NSR-related lantibiotic resistance by small molecules.

# **Conflict of interest**

The authors confirm that this article content has no conflict of interest.

# Acknowledgements

This study was funded by the Deutsche Forschungsgemeinschaft (DFG, German Research Foundation) – 270650915 (Research Training Group GRK 2158, TP4a to HG and SS, TP1d to HS and an Emmy Noether grant ET 102/2-1 to ME). We are grateful for computational support by the "Zentrum für Informations und Medientechnologie" at the Heinrich-Heine-Universität Düsseldorf and the computing time provided by the John von Neumann Institute for Computing (NIC) to HG and BF on the supercomputer JURECA at Jülich Supercomputing Centre (JSC) (user ID: HKF7). Funding by Deutsche Forschungsgemeinschaft (DFG) (INST 208/704-1 FUGG) to purchase the hybrid computer cluster used in this study is gratefully acknowledged. The authors acknowledge access to the Jülich-Düsseldorf Biomolecular NMR Center that is jointly run by Forschungszentrum Jülich and Heinrich-Heine-Universität Düsseldorf. The Center for Structural Studies is funded by the Deutsche Forschungsgemeinschaft (DFG Grant number 417919780).

#### **Author contribution**

HG and SS conceived and supervised the study; NP and BF performed *in silico* screening; JZK performed *in vivo* assays; MG performed and analyzed STD NMR measurements, and ME contributed to the analysis; AZ performed LC-MS purity assessment; NP performed MD simulations; NP and HG wrote the manuscript; JZK, SS, and HS contributed to the writing.

# **Supplementary Material**

Supplementary data associated with this article can be found in Supporting Information.

# References

- 1. Chen, L., et al., *Notes from the Field: Pan-Resistant New Delhi Metallo-Beta-Lactamase-Producing Klebsiella pneumoniae Washoe County, Nevada, 2016.* MMWR Morb Mortal Wkly Rep, 2017. **66**(1): p. 33.
- 2. Sahl, H.G. and G. Bierbaum, *Lantibiotics: biosynthesis and biological activities of uniquely modified peptides from gram-positive bacteria*. Annu Rev Microbiol, 1998. **52**: p. 41-79.
- 3. Dischinger, J., S. Basi Chipalu, and G. Bierbaum, *Lantibiotics: Promising candidates for future applications in health care.* Int J Med Microbiol, 2014. **304(1)**: p. 51-62.
- 4. Oppedijk, S.F., N.I. Martin, and E. Breukink, *Hit 'em where it hurts: The growing and structurally diverse family of peptides that target lipid-II.* BBA Biomemb, 2016. **1858(5)**: p. 947-957.
- 5. Shin, J.M., et al., *Biomedical applications of nisin*. J Appl Microbiol, 2016. **120(6)**: p. 1449-1465.
- 6. Rogers, L.A. and E.O. Whittier, *Limiting Factors in the Lactic Fermentation*. J Bacteriol, 1928. **16**(4): p. 211-29.
- 7. Delves-Broughton, J., et al., *Applications of the bacteriocin, nisin*. Antonie Van Leeuwenhoek, 1996. **69**(2): p. 193-202.
- 8. Hasper, H.E., et al., *An alternative bactericidal mechanism of action for lantibiotic peptides that target lipid II.* Science, 2006. **313**(5793): p. 1636-7.
- 9. Wiedemann, I., et al., Specific binding of nisin to the peptidoglycan precursor lipid II combines pore formation and inhibition of cell wall biosynthesis for potent antibiotic activity. J Biol Chem, 2001. **276**(3): p. 1772-9.
- 10. Hsu, S.T., et al., *The nisin-lipid II complex reveals a pyrophosphate cage that provides a blueprint for novel antibiotics.* Nat Struct Mol Biol, 2004. **11**(10): p. 963-7.
- 11. Khosa, S., Z. Alkhatib, and S.H. Smits, *NSR from Streptococcus agalactiae confers resistance against nisin and is encoded by a conserved nsr operon.* Biol Chem, 2013. **394**(11): p. 1543-9.
- 12. Froseth, B.R. and L.L. McKay, *Molecular characterization of the nisin resistance region of Lactococcus lactis subsp. lactis biovar diacetylactis DRC3*. Appl Environ Microbiol, 1991. **57**(3): p. 804-11.
- 13. Rawlings, N.D., et al., *The MEROPS database of proteolytic enzymes, their substrates and inhibitors in 2017 and a comparison with peptidases in the PANTHER database.* Nucleic Acids Research, 2018. **46**(D1): p. D624-D632.
- 14. Sun, Z., et al., *Novel mechanism for nisin resistance via proteolytic degradation of nisin by the nisin resistance protein NSR*. Antimicrob Agents Chemother, 2009. **53**(5): p. 1964-73.
- 15. Khosa, S., et al., Structural basis of lantibiotic recognition by the nisin resistance protein from Streptococcus agalactiae. Sci Rep, 2016. **6**.
- 16. Schrödinger Release 2017-1: Schrödinger Suite 2017-1 Protein Preparation Wizard, Schrödinger, LLC, New York, NY, 2017.
- 17. Banks, J.L., et al., *Integrated Modeling Program, Applied Chemical Theory (IMPACT)*. J Comput Chem, 2005. **26**(16): p. 1752-80.
- 18. Case, D.A., et al., AMBER 2016. 2016: Uiversity of California, San Francisco.
- 19. Roe, D.R. and T.E. Cheatham, 3rd, *PTRAJ and CPPTRAJ: Software for Processing and Analysis of Molecular Dynamics Trajectory Data.* J Chem Theory Comput, 2013. **9**(7): p. 3084-95.
- 20. Hawkins, P.C., A.G. Skillman, and A. Nicholls, *Comparison of shape-matching and docking as virtual screening tools.* J Med Chem, 2007. **50**(1): p. 74-82.
- 21. Sterling, T. and J.J. Irwin, *ZINC 15--Ligand Discovery for Everyone*. J Chem Inf Model, 2015. **55**(11): p. 2324-37.
- 22. Hawkins, P.C., et al., Conformer generation with OMEGA: algorithm and validation using high quality structures from the Protein Databank and Cambridge Structural Database. J Chem Inf Model, 2010. **50**(4): p. 572-84.
- 23. Schrödinger Release 2017-1: Schrödinger Suite 2017-1 Glide, Schrödinger, LLC, New York, NY, 2017.
- 24. Schrödinger Release 2017-1: Schrödinger Suite 2017-1 Canvas, S., LLC, New York, NY, 2017.

- 25. Oprea, T.I., et al., *Is There a Difference between Leads and Drugs? A Historical Perspective.* J Chem Inf Comput Sci, 2001. **41(5)**: p. 1308-1315.
- 26. Frisch, M.J., et al., Gaussian 16, Revision B.01. 2016, Gaussian, Inc.: Wallingford CT.
- 27. Bayly, C.I., et al., A Well-Behaved Electrostatic Potential Based Method Using Charge Restraints for Deriving Atomic Charges the Resp Model. J Phys Chem, 1993. **97(40)**: p. 10269-10280.
- 28. Wang, J., et al., Automatic atom type and bond type perception in molecular mechanical calculations. J Mol Graph Model, 2006. **25**(2): p. 247-60.
- 29. Schafmeister CEAF, Ross WS, Romanovski V. LEaP. University of California, San Francisco: 1995.
- 30. Martinez, L., et al., *PACKMOL*: a package for building initial configurations for molecular dynamics simulations. J Comput Chem, 2009. **30**(13): p. 2157-64.
- 31. Jorgensen, W.L., et al., *Comparison of Simple Potential Functions for Simulating Liquid Water.* J Chem Phys, 1983. **79(2)**: p. 926–35.
- 32. Salomon-Ferrer, R., et al., *Routine Microsecond Molecular Dynamics Simulations with AMBER on GPUs. 2. Explicit Solvent Particle Mesh Ewald.* J Chem Theory Comput, 2013. **9**(9): p. 3878-88.
- 33. Maier, J.A., et al., ff14SB: Improving the Accuracy of Protein Side Chain and Backbone Parameters from ff99SB. J Chem Theory Comput, 2015. 11(8): p. 3696-713.
- Wang, J., et al., *Development and testing of a general amber force field.* J Comput Chem, 2004. **25**(9): p. 1157-74.
- 35. Joung, I.S. and T.E. Cheatham, 3rd, *Determination of alkali and halide monovalent ion parameters for use in explicitly solvated biomolecular simulations*. J Phys Chem B, 2008. **112**(30): p. 9020-41.
- 36. Frieg, B., et al., Molecular Mechanisms of Glutamine Synthetase Mutations that Lead to Clinically Relevant Pathologies. PLoS Comput Biol, 2016. **12**(2): p. e1004693.
- 37. Holo, H. and I.F. Nes, *High-Frequency Transformation, by Electroporation, of Lactococcus lactis subsp. cremoris Grown with Glycine in Osmotically Stabilized Media.* Appl Environ Microbiol, 1989. **55**(12): p. 3119-23.
- 38. Khosa, S., et al., *Overexpression, purification, crystallization and preliminary X-ray diffraction of the nisin resistance protein from Streptococcus agalactiae*. Acta Crystallogr F Struct Biol Commun, 2015. **71**(Pt 6): p. 671-5.
- 39. Abts, A., et al., Easy and rapid purification of highly active nisin. Int J Pept, 2011. **2011**: p. 175145.
- 40. Abts, A., et al., *NisC binds the FxLx motif of the nisin leader peptide*. Biochemistry, 2013. **52**(32): p. 5387-5395.
- 41. Reiners, J., et al., *The N-terminal Region of Nisin Is Important for the BceAB-Type ABC Transporter NsrFP from Streptococcus agalactiae COH1*. Front Microbiol, 2017. **8**: p. 1643.
- 42. Mayer, M. and B. Meyer, *Group epitope mapping by saturation transfer difference NMR to identify segments of a ligand in direct contact with a protein receptor.* J Am Chem Soc, 2001. **123**(25): p. 6108-17.
- 43. Mayer, M. and B. Meyer, *Characterization of Ligand Binding by Saturation Transfer Difference NMR Spectroscopy*. Angew Chem Int Ed Engl, 1999. **38**(12): p. 1784-1788.
- 44. Patani, G.A. and E.J. LaVoie, *Bioisosterism: A Rational Approach in Drug Design*. Chem Rev, 1996. **96**(8): p. 3147-3176.
- 45. Graham, T.H., et al., *Pyrazoles as non-classical bioisosteres in prolylcarboxypeptidase (PrCP) inhibitors.* Bioorg Med Chem Lett, 2014. **24**(7): p. 1657-60.
- 46. Eisenberg, D., R.M. Weiss, and T.C. Terwilliger, *The hydrophobic moment detects periodicity in protein hydrophobicity*. Proc Natl Acad Sci U S A, 1984. **81**(1): p. 140-4.
- 47. Buch, I., T. Giorgino, and G. De Fabritiis, *Complete reconstruction of an enzyme-inhibitor binding process by molecular dynamics simulations*. Proc Natl Acad Sci U S A, 2011. **108**(25): p. 10184-9.
- 48. Xia, Y., et al., Clean STD-NMR spectrum for improved detection of ligand-protein interactions at low concentration of protein. Magn Reson Chem, 2010. **48**(12): p. 918-24.
- 49. *ChEMBL database (accessed on April 23rd 2019).*